JOURNAL OF AIRCRAFT
Vol. 29, No. 2, March–April 1992

Experimental Study of a Low Reynolds Number Tandem Airfoil Configuration

Daniel F. Scharpf* and Thomas J. Mueller†
University of Notre Dame, Notre Dame, Indiana 46556

Experiments were concluded with two identical Wortmann FX63-137 airfoils in closely coupled tandem configurations at a Reynolds number of 8.5 × 10⁴. For the data presented here, the values of the stagger and gap were 1.5 and 0, respectively. The decalage angles were 0 and ±10 deg. Direct measurement of lift, drag, and 1/4-chord pitching moment, as well as static pressure distributions, were acquired for each airfoil. Flow visualization using kerosene smoke was performed to complement the experimental data. The total drag reduction and lift increase resulted in a significant increase in the lift-to-drag ratio for a number of configurations.

Nomenclature

A_w = wing area
C_d = section drag coefficient, $D/(A_w q_\infty)$
C_l = section lift coefficient, $L/(A_w q_\infty)$
C_m = section 1/4-chord moment coefficient, $M/(cA_w q_\infty)$
C_p = pressure coefficient, $1-q/q_\infty$
c = chord length
D = drag force
G = gap, $|y|/c$
L = lift force
M = 1/4-chord pitching moment
q = dynamic pressure, $\frac{1}{2}\rho U^2$
R_c = Reynolds number based on chord, $U_\infty c/\nu$
St = stagger, x/c (positive when upstream airfoil is above the downstream airfoil)
U = flow velocity
x = distance in streamwise direction
y = distance normal to streamwise directions
α = angle of attack
δ = decalage, $\alpha_{ua} - \alpha_{da}$

Subscripts
da = downstream airfoil
s = single airfoil
tot = combination of wing and canard
ua = upstream airfoil
1/4 = quarter chord
∞ = freestream condition

Introduction

AERODYNAMICS at low Reynolds numbers has become a field of increasing interest in recent years. This is primarily due to the expanding applications in remotely piloted vehicles (RPVs), ultralight aircraft, human powered aircraft, and wind turbines.[1] The resurgence of low Reynolds number airfoil aerodynamics, combined with the recent interest in the viability of canard and tandem wing aircraft,[2] is the basis for the present research. Most of the current numerical and experimental research involving these multisurface configurations is in the Reynolds number range above 10^6. This is primarily due to the fact that this is the region where conventional aircraft operate, with the exception of mini-RPVs. Therefore, in order to assess the performance characteristics of these configurations at Reynolds numbers $< 5 \times 10^5$, experimental data was desired.

Most experimental studies that have been performed on multiwing systems concerned finite span wings, which, therefore, includes the effect of the tip vortices on the performance of each of the wings. The experiments performed by Feistal et al.[3] were performed at a Reynolds number of 1.4×10^6 for a set of finite span wings. The results showed that the interference for some configurations was favorable for the canard (increased $C_{L\max}$), with no decrease in the maximum lift coefficient of the wing. Experiments dealing with three-dimensional biplane wing configurations by Olson and Selberg[4] showed improved performance over a comparable monoplane configuration. This work, however, was performed at a Reynolds number of 8.7×10^5, which does not include the low Reynolds number effects that are typical for values of $Re < 5 \times 10^5$, e.g., large transitional separation bubbles. Current research at low Reynolds numbers includes work done by Michelson and Mueller[5] in which measurements were performed on dual wing systems for $R_c = 1.5 \times 10^5$. The downstream airfoil in these experiments was situated between two end plates, which isolated it from the tip vortices of the canard. This tip vortex has been shown to contribute favorably to the aerodynamics of the system for certain configurations.[6,7]

Analytical techniques have been used by numerous researchers in an effort to determine the benefits or drawbacks from using these multisurface configurations.[8–12] It has been found by these researchers that a decrease in the overall drag of the system, compared to the single wing case, can be obtained for appropriate configurations. Again, it must be stressed that these too have been performed at Reynolds numbers well above 5×10^5. At Reynolds numbers in this range, leading-edge separation bubbles are very small, or nonexistent. The difficulty with modeling flows at lower Reynolds numbers ($R_c < 5 \times 10^5$) stems from the fact that in this regime the separation bubble can be quite large, thus having a dramatic effect on the aerodynamics of the airfoil.

The studies that are performed in the present research were designed to examine the performance characteristics of two tandem Wortmann FX63-137 airfoils. The parameters used to describe the configuration of the airfoils are the stagger, gap, and decalage, as shown in Fig. 1.

Flow Character of the Wortmann FX63-137

At low speeds ($Rc < 5 \times 10^5$), a laminar separation bubble can form on the airfoil. The separation bubble begins to form

Received July 11, 1990; Presented as Paper 90-3094 at the AIAA 8th Applied Aerodynamics Conference, Portland, OR, Aug. 20–22, 1990; revision received March 19, 1991; accepted for publication April 6, 1991. Copyright © 1990 by Thomas J. Mueller. Published by the American Institute of Aeronautics and Astronautics, Inc., with permission.

*Graduate Research Assistant, Department of Aerospace and Mechanical Engineering. Member AIAA.
†Roth-Gibson Professor, Department of Aerospace and Mechanical Engineering. Associate Fellow AIAA.

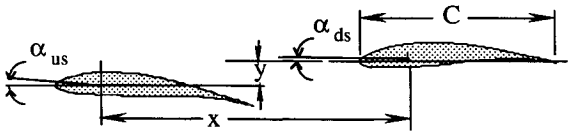

Fig. 1 Tandem-airfoil configuration parameters.

when the laminar boundary layer near the leading edge of the airfoil cannot overcome the adverse pressure gradient due to the curvature of the airfoil. This results in a free shear layer that transitions from a laminar to a turbulent flow, therefore adding enough energy to the flow near the surface so that it is now capable of reattaching as a turbulent boundary layer. The region bounded by the point of separation, the free shear layer, and the point of reattachment is known as the separation bubble. Numerous researchers have documented this phenomenon and have shown how its existence can drastically effect the performance of the airfoil.[13,14] At low Reynolds numbers, the length of the bubble may extend more than 40% of the chord, effectively changing the profile of the airfoil and resulting in conditions that may not have been anticipated in the original airfoil design.

For Reynolds numbers above 10^6, transition from a laminar to a turbulent boundary layer usually occurs without separation. Therefore, for most high Reynolds number airfoil applications, the separation bubble is not a problem. However, at the low Reynolds numbers, as in the present investigation, the separation bubble plays a dominant role.

Apparatus and Procedure

All of the experiments were performed in the south subsonic wind tunnel at the University of Notre Dame Aerospace Laboratory. This tunnel is an open circuit, atmospheric exhaust type. The inlet has a 10- × 10-ft (3.04- × 3.04-m) square cross section and has an area contraction ratio of 24:1, which permits a 2- × 2-ft (0.61- × 0.61-m) working test section. The level of turbulence intensity for the tunnel is <0.08% for a frequency bandwidth from 1 to 2500 Hz. The tunnel velocity for the results presented here was 29 ft/s (9 m/s).

In order to reduce wingtip effects and subject the downstream airfoil to only the wake of the upstream airfoil, both airfoils were mounted between one set of end plates. Both airfoils had a 6-in. chord and a 16-in. span. The gap between the ends of the airfoils and the end plates was maintained at 0.02 in.[15,16] This arrangement minimized the spanwise variation of aerodynamic loads experienced by the airfoils so that a two-dimensional flow was approximated. The results presented here concern two identical rectangular platform airfoils with the Wortmann FX63-137 profile.

Several configurations and Reynolds numbers were examined in the investigation that gave rise to the focus on the data presented here. All combinations of $St = \pm 2$ and ± 1.5, $G = 0$ and 1, and $R_c = 8.5 \times 10^4$ and 2×10^5 were performed. Significant results from the measurements showed a decrease in the aerodynamic influence for $St = \pm 2$ and gaps of 1. At a Reynolds number of 2×10^5, the downwash from the upstream airfoil appeared to be the most significant factor in altering the performance of the downstream airfoil. The lift and drag on the rearward airfoil decreased and increased, respectively, for all configurations at this Reynolds number, resulting in a loss of performance for all configurations. The data presented here reflects the configurations for which the aerodynamic interaction was most dramatic, i.e., $R_c = 8.5 \times 10^4$, $St = 1.5$, and $G = 0$.

The force measurements were made using a three-component force balance capable of measuring lift, drag, and 1/4-chord pitching moment.[17] Both airfoils were mounted vertically in the test section, allowing aerodynamic force measurement of a single airfoil. The airfoil attached to the balance was rotated in angle of attack from −15 to 20 deg and back to 0 deg in order to record any aerodynamic hysteresis effects. The force data was then ensemble averaged with at least three data sets for each test configuration. Maximum error in measured values of $C_{l\max}$ and $C_{d\min}$ were calculated to be 2.6 and 5.8%,[17] respectively.

A separate airfoil model outfitted with 40 pressure taps was used to obtain the surface pressure distributions. Twenty five ports were on the upper surface and 15 were on the lower surface, with a concentration of taps near the leading edge. The taps were staggered slightly in the spanwise direction so that any disturbance caused by an upstream tap would not influence the measurement at a subsequent location. The pressure measurements were performed with both airfoils mounted in cantilever fashion for fixed values of both α_{ua} and α_{da}. The pressure distributions on both airfoils were found for all combinations of α_{ua} and $\alpha_{da} = 0$, 5, and 10 deg. Maximum error in the measured values of pressure coefficient was 4.17% at $C_{p\max}$.[17]

Flow visualization using kerosene smoke was performed to complement the quantitative data. This provided some insight to the physics of the flow and facilitated analysis of the force and pressure data. A complete description of the flow visualization apparatus may be found in Ref. 15.

Results

Flow Visualization Results

Arranging the airfoils in this closely coupled arrangement not only influenced the aerodynamic forces experienced by each airfoil, but it also affected the range of Reynolds numbers where the separated-flow hysteresis occurred. The Wortmann FX63-137 airfoil was designed for low-speed applications,[18] i.e., $2.5 \times 10^5 < R_c < 4 \times 10^6$. In this region and below, the viscous effects tend to dominate the flow character. It was found that when accelerating from a zero base velocity at an angle of attack of 5 deg the flow over the airfoil is initially separated and does not attach to the upper surface of the airfoil until a Reynolds of 8.7×10^4 is reached. When the incidence is increased to 10 deg, the attachment occurs at $R_c \approx 8.2 \times 10^4$. The flow will remain attached as long as the freestream speed is increased. The hysteresis effects occur when the flow is decelerated after attachment has occurred. The flow will separate from the airfoil at $R_c = 8.6 \times 10^4$ and 5.6×10^4 for angles of attack of 5 and 10 deg, respectively. Therefore, two distinct flow structures are possible for the same Reynolds number within these hysteresis regions.

When a second airfoil is introduced, as in the tandem arrangement, the range of these separated-flow hysteresis regions increases. These regions are a function of the angles of attack of each airfoil and the streamwise distance between them. The flow character over the forward airfoil was indicative of the flow over the rearward airfoil, i.e., separated or attached flow over the upstream airfoil resulted in the same flow structure over the downstream airfoil. Figure 2 is a composite sketch of the overall separated-flow hysteresis regions for airfoil angles of 5 and 10 deg and staggers of 1.5 and 2, with a gap of 0. The graph can be interpreted in the following fashion. For $\alpha_{ua} = 5$ deg, the flow is separated until a Reynolds number of 9.7×10^4 is reached. Beyond this speed, the flow remains attached. Decreasing the Reynolds number

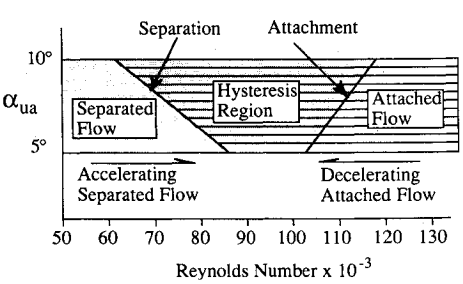

Fig. 2 Separated-flow hysteresis regions for tandem airfoils.

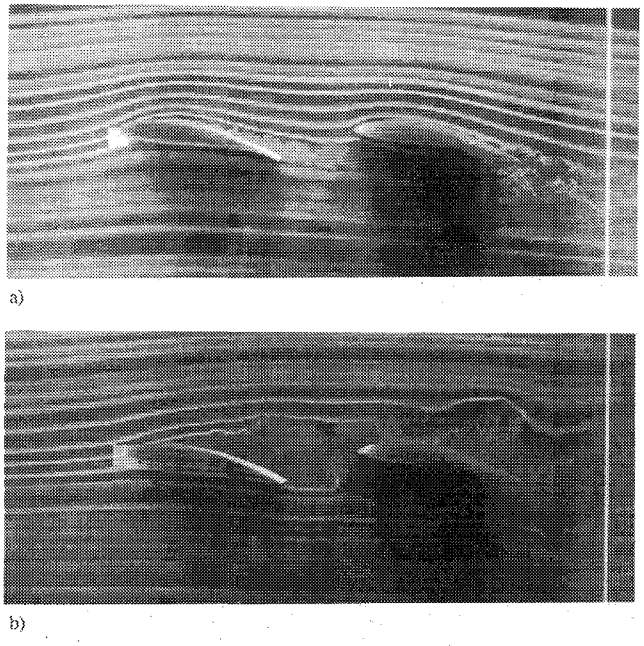

Fig. 3 Tandem airfoils at $R_c = 8.5 \times 10^4$, illustrating the separation hysteresis phenomenon for $\alpha_{ua} = \alpha_{da} = 10$ deg: a) attached-flow condition; b) separated-flow condition ($St = 1.5$, $G = 0$, $\delta = 0$ deg).

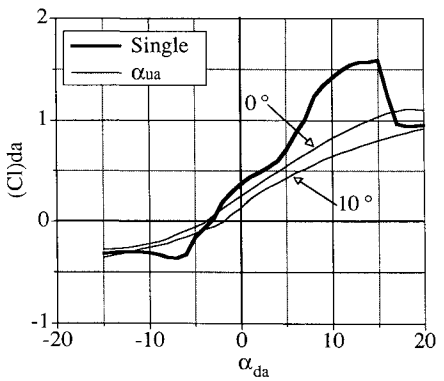

Fig. 4 Lift coefficient of downstream airfoil for $\alpha_{ua} = 0$ and 10 deg ($St = 1.5$, $G = 0$).

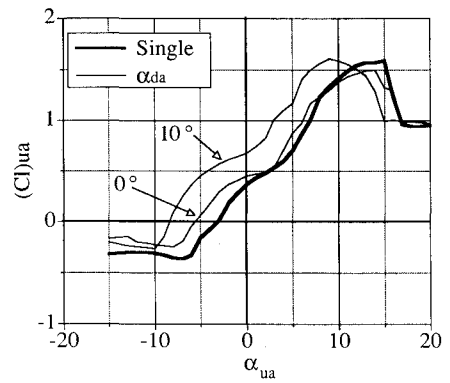

Fig. 5 Lift coefficient of upstream airfoil for $\alpha_{da} = 0$ and 10 deg ($St = 1.5$, $G = 0$).

results in separation occurring at $R_c = 8.2 \times 10^4$, thus generating a hysteresis region between Reynolds numbers of 8.2×10^4 and 9.7×10^4. A similar account occurs for $\alpha_{ua} = 10$ deg, except that the resulting hysteresis region is larger.

The hysteresis can be explained as follows. When the flow begins from very low speeds, there is not enough energy in the flow to overcome the adverse pressure gradient caused by the upper surface of the forward airfoil. As the speed is increased, the energy in the flow is increased until sufficient energy exists such that the flow can negotiate the adverse pressure gradient. Once this occurs, the flow remains attached. By decreasing the speed of the flow, the energy also decreases. The ability of the flow to remain attached at a Reynolds number below which attached flow was not previously seen appears to be a result of an increased stability inherent with the attached condition. The difference in the Reynolds numbers where attachment and separation occur may also be due to the *apparent* shape of the airfoil when the flow is separated; i.e., the approach flow sees the airfoil as a bluff body due to the large separated flow region. The presence of the downstream airfoil increased the hysteresis region of the single airfoil by contributing to the streamwise pressure difference between the leading- and trailing-edge of the upstream airfoil.

A trend that is apparent from Fig. 2 is that the flow needs to be at a higher Reynolds number for attachment to occur when $\alpha_{ua} = 10$ deg. The increase in the angle of attack results in an increased adverse pressure gradient, thus requiring more energy for attachment to occur. This increased pressure gradient appears to add to the stability of the attached flow condition as evidenced by the lower separation Reynolds number at this higher angle of attack.

Figures 3a and 3b are flow visualization photographs of the tandem wings at $R_c = 8.5 \times 10^4$ for the attached- and separated-flow conditions, respectively. It is important to note that the Reynolds number at which the force and pressure measurements were taken occur in this hysteresis region. Because of this, it was necessary to be aware of the flow condition that was present during acquisition. For all data shown here, the attached-flow condition existed.

Force Measurement Results

Force data was acquired for one of the airfoils while the second was held at a constant angle of attack of 0, 5, or 10 deg. This resulted in a series of force coefficient curves for the measured airfoil for constant angles of attack of the second airfoil. From these data, the complementary force coefficients from each case were added to give the combined effect of the tandem airfoils. These combined and individual results were compared to a baseline case consisting of a single airfoil under the same conditions as the tandem airfoil arrangement. In the following plots and discussion, the case for a fixed airfoil at $\alpha_{ua,\,da} = 5$ deg is omitted for clarity. This configuration was generally an intermediate step in the trends seen from changing α from 0 to 10 deg.

By introducing an upstream airfoil into the flow, the lift coefficient of the rearward airfoil decreased from the single-airfoil baseline case for most values of α_{da} and all values of α_{ua}. The single airfoil was seen to stall at $\alpha_s = 16$ deg, whereas the introduction of the upstream airfoil resulted in attached flow on the rearward airfoil for all angles of attack measured. This was the result of the decrease in the effective angle of

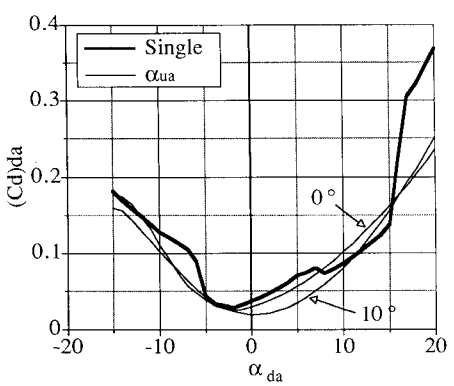

Fig. 6 Drag coefficient of downstream airfoil for $\alpha_{ua} = 0$ and 10 deg ($St = 1.5$, $G = 0$).

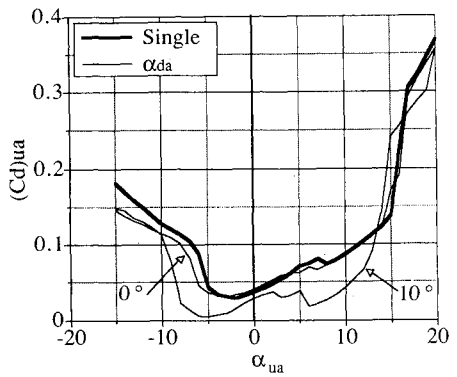

Fig. 7 Drag coefficient of upstream airfoil for α_{da} = 0 and 10 deg (St = 1.5, G = 0).

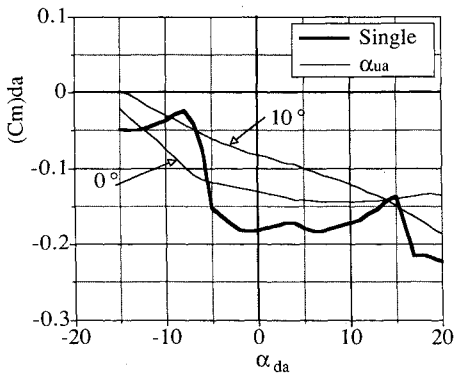

Fig. 8 1/4-chord moment coefficient of downstream airfoil for α_{ua} = 0 and 10 deg (St = 1.5, G = 0).

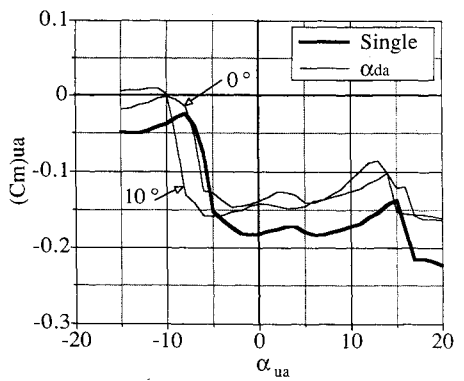

Fig. 9 1/4-chord moment coefficient of upstream airfoil for α_{da} = 0 and 10 deg (St = 1.5, G = 0).

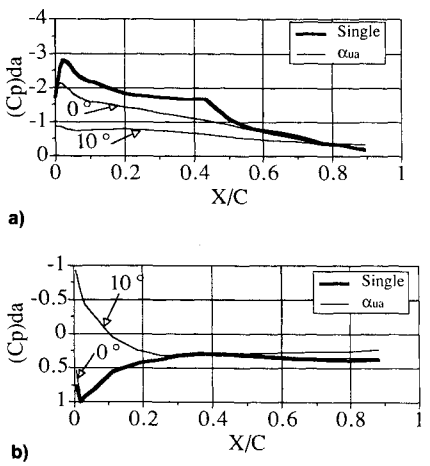

Fig. 10 Pressure distribution on downstream airfoil for α_{da} = 10 deg and α_{ua} = 0 and 10 deg: a) upper surface; b) lower surface (St = 1.5, G = 0, δ = 10, 0 deg).

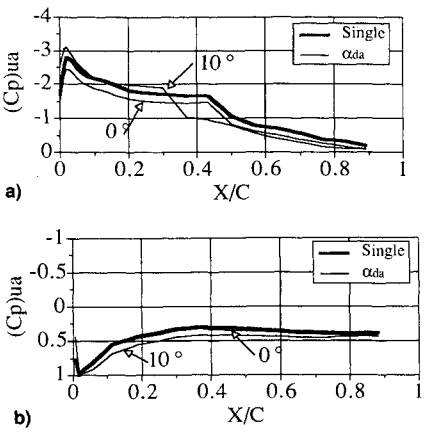

Fig. 11 Pressure distribution on upstream airfoil for α_{ua} = 10 deg and α_{da} = 0 and 10 deg: a) upper surface; b) lower surface (St = 1.5, G = 0, δ = 10, 0 deg).

attack of the downstream airfoil due to the downwash of the upstream airfoil. From the flow visualization, the wake of the forward airfoil travels below the downstream airfoil when the attached flow condition exists. This low-pressure region below the wing also contributes to the loss in lift experienced by the downstream airfoil (see Fig. 4). The forward airfoil in the tandem case was seen to have an increase in the lift coefficient over the single airfoil. This was most evident for α_{da} = 10 deg (see Fig. 5). The reason for this will be seen from the results of the canard pressure distributions. The influence of the upstream airfoil on the value of $(C_d)_{da}$ resulted in a lower drag for most values of α_{da}, as seen in Fig. 6.

By delaying the onset of stall, the drag at high values of α_{da} was reduced by as much as 27%. For α_{da} = 5 deg and α_{ua} = 10 deg, the reduction in $(C_d)_{da}$ was 48%. It should be noted, however, that the true drag coefficient should be referenced to the local dynamic pressure, and since the wing is operating near the wake of the upstream airfoil, q_{local} will be $> q_\infty$, thereby increasing $(C_d)_{da}$. The decrease in $(C_d)_{da}$ can, therefore, be seen as a decrease in the drag force. The addition of the downstream airfoil drastically decreased the drag of the forward airfoil, with the largest influence occurring for α_{da} = 10 deg (see Fig. 7). This decrease in $(C_d)_{ua}$ can be explained by the increase in the static pressure between the airfoils, which effectively reduces the streamwise pressure difference between the leading- and trailing-edge of the upstream airfoil. This phenomenon can be so strong in some cases that a thrust can be generated on the upstream airfoil.[19] The moment coefficients for each airfoil showed a general increase for most α_{ua} values, putting the downstream airfoil closer to an unstable arrangement, i.e., $C_m > 0$ (see Figs. 8 and 9). This shows that the influence of each airfoil on the other tends to move the net aerodynamic force toward its respective 1/4-chord location.

Pressure Measurement Results

The location of the separation bubble (if it exists) can be extracted from the pressure distributions. The beginning of the bubble is the point at which a plateau region begins in the pressure distribution: a result of the recirculating fluid within the bubble. The transition location is identified by a sharp increase in pressure from the plateau region. The bubble then ends where the pressure distribution would have been if the bubble were not present. This location is quite subjective when determining the location of the end of the bubble from pressure profiles. The most interesting effects of having two airfoils in the flow can be seen in the pressure profiles for α_{da} and α_{ua} = 10 deg. Figures 10a and 10b show a comparison between the single airfoil pressure profile and the profiles on the downstream airfoil when the forward airfoil is at 0 and 10 deg. The significant drop in lift seen in the force measurement under these conditions is a direct result of the de-

Table 1 Force coefficients for tandem- and single-airfoil measurements (St = 1.5, G = 0, $R_c = 8.5 \times 10^4$)

Incidence		C_l		C_d		L/D	
δ, deg	$\alpha_{ua,\,da}$, deg	s	tot	s	tot	s	tot
−10	10	1.383	1.502	0.082	0.130	16.776	11.554
− 5	5	0.686	1.077	0.065	0.095	10.507	11.337
− 5	10	1.383	2.206	0.082	0.137	16.776	16.102
0	0	0.359	0.700	0.032	0.070	11.088	10.000
0	5	0.686	1.729	0.065	0.106	10.507	16.311
0	10	1.383	2.223	0.082	0.123	16.776	18.073
5	0	0.359	1.199	0.032	0.089	11.088	13.472
5	5	0.686	1.975	0.065	0.106	10.507	18.632
10	0	0.359	1.515	0.032	0.108	11.088	14.028

crease in the pressure difference across the surfaces of the downstream airfoil. The separation bubble that exists on the single airfoil from approximately 20 to 55% chord extends only about 10% of the chord for α_{ua} = 0 deg and does not even exist when α_{ua} = 10 deg. The rearward airfoil for the latter case exhibits stall characteristics. The decrease in the size of the separation bubble results in a decrease in the form drag, but it also indicates that a turbulent boundary layer exists over a greater portion of the airfoil, which will tend to increase the skin friction drag. The overall result from the force measurement is a slight increase in the drag for α_{da} = 10 deg and α_{ua} = 0 deg.

The pressure distribution over the upstream airfoil for α_{ua} = 10 deg and α_{da} = 0 and 10 deg is shown in Fig. 11. From this figure it can be seen that the pressure on the upper surface of the forward airfoil has increased, whereas the pressure on the lower surface has remained relatively unaltered for α_{da} = 0 deg. The result is a slight decrease in the lift of the upstream airfoil. The length and the position of the separation bubble has not been affected by the introduction of the downstream airfoil at 0 deg. When α_{da} = 10 deg, however, the increased static pressure from the rearward airfoil becomes apparent. The length of the separation bubble is decreased most likely because of the decrease in the pressure gradient over the upper surface of the forward airfoil. The lower surface of this airfoil experiences an increase in static pressure. These two factors contribute to the increased lift that was seen in the force measurements. The change in the flow character around the upstream airfoil is primarily due to the pressure difference caused by the presence of the downstream airfoil. Because of this, the decrease in the $(C_d)_{ua}$ is most likely the result of the decrease in the form drag and not a decrease in the skin friction.

Conclusions

Comparison of the combined tandem-airfoil performance to the single-airfoil performance is shown in Table 1. Decalage values are compared to the single-airfoil case for equal values of α_{da} and α_s. For the same decalage angle, a variety of performance coefficients result. This indicates that, whereas the *relative* angle of attack between the two airfoils may be the same, the incidence of each airfoil with respect to the freestream is also important. Since all of the force coefficients are referenced to the same freestream dynamic pressure, the total force coefficient for the tandem wing case is merely the sum of the individual force coefficients. The total lift-to-drag ratio is then $(L/D)_{tot} = [(C_l)_{tot}]/[(C_d)_{tot}]$. A comparison between a single airfoil is made since the original objective was to determine if any benefits could be gained from using a tandem-airfoil configuration over a single-airfoil configuration. Although in all cases the combined lift and drag coefficients were greater than the single wing coefficients, their combined lift to drag ratios varied. The greatest improvement occurs for α_s = 5 deg. The largest improvement was an increase in L/D of 77%, which occurred for α_{da} = 5 deg and α_{ua} = 10 deg. It can also be seen from Table 1 that an increase in L/D occurred for all values of positive decalage ($\delta = \alpha_{ua} - \alpha_{da}$). For decalages of 0 deg, a decrease in L/D was only seen for $\alpha_{ua} = \alpha_{da} = 0$ deg.

Since increased performance is unique to the requirements of the application, the benefits or disadvantages of using any of these configurations will correspond solely to each specific design requirement. Therefore, one cannot simply say that one configuration is better than another, except when a specific performance requirement is identified. The results do, however, show that some advantages over a single-wing design can be gained by utilizing a closely coupled tandem-wing arrangement. It should also be noted that these results are independent of tip vortex effects produced by finite wings.

Acknowledgments

This research was conducted in the Aerospace Laboratory of the University of Notre Dame and supported by the Department of Aerospace and Mechanical Engineering and the U.S. Navy Office of Naval Research under Contract N00014-83-K-0239.

References

[1]Mueller, T. J., "Low Reynolds Number Vehicles," AGARDograph No. 288, Feb. 1985.

[2]Rutan, B., "Tale of Three EZ's," *Sport Aviation*, Vol. 29, No. 2, 1980, 34–39.

[3]Feistal, T. W., Corsiglia, V. R., and Levin, D. B., "Wind Tunnel Measurements of Wing-Canard Interference and a Comparison with Various Theories," Society of Automotive Engineers, Paper 810575, Vol. 90, Sec. 2, April 1981, pp. 2026–2039.

[4]Olson, E. C., and Selberg, B. P., "Experimental Determination of Improved Aerodynamic Characteristics Utilizing Biplane Wing Configurations," *Journal of Aircraft*, Vol. 13, No. 4, 1976, pp. 256–261.

[5]Michelson, W. D., and Mueller, T. J., "Low Reynolds Number Airfoil Performance Subjected to Wake Interference From an Upstream Airfoil," AIAA Paper 87-2351, AIAA 5th Applied Aerodynamics Conference, Monterey, CA, Aug. 1987.

[6]Khan, F. A., and Mueller, T. J., "Tip Vortex/Airfoil Interaction for a Canard/Wing Configuration at Low Reynolds Numbers," AIAA Paper 89-0536, 27th Aerospace Sciences Meeting, Reno, NV, Jan. 1989.

[7]Walker, J. M., and Robinson, M. C., "Impingement of Orthogonal Unsteady Vortex Structures on Trailing Aerodynamic Surfaces," AIAA Paper 88-2580, AIAA 6th Applied Aerodynamics Conference, Williamsburg, VA, 1988, pp. 463–472.

[8]Laitone, E. V., "Prandtl's Biplane Theory Applied to Canard and Tandem Wing Aircraft," *Journal of Aircraft*," Vol. 17, No. 4, 1980, pp. 233–237.

[9]Prandtl, L., "Induced Drag of Multiplanes," NACA TN-182, March 1924.

[10]Rhodes, M. D., and Selberg, B. P., "Benefits of Dual Wings over Single Wings for High-Performance Business Airplanes," *Journal of Aircraft*, Vol. 21, No. 2, 1984, pp. 116–127.

[11]Selberg, B. P., and Rokhsaz, K., "Aerodynamic Tradeoff Study of Conventional, Canard, and Trisurface Aircraft Systems," *Journal of Aircraft*, Vol. 23, No. 10, 1986, pp. 629–630.

[12]Addoms, R. B., and Spaid, F. W., "Aerodynamic Design of High Performance Biplane Wings," *Journal of Aircraft*, Vol. 12, No. 8, 1975.

[13]Tani, I., "Low Reynolds Number Flows Involving Bubble Sep-

arations," *Progress in Aeronautical Sciences*, Vol. 5, 1964, pp. 71–103.

[14]O'Meara, M. M., and Mueller, T. J., "Laminar Separation Bubble Characteristics on an Airfoil at Low Reynolds Numbers," *AIAA Journal*, Vol. 25, No. 8, 1987, pp. 1033–1041.

[15]Mueller, T. J., et al., "Low Reynolds Number Wind Tunnel Measurements: The Importance of Being Earnest," *Proceedings of the International Conference on Aerodynamics at Low Reynolds Numbers*, London, England, Vol. 2, Oct. 1986.

[16]Pope, A., and Harper, J. J., *Low Speed Wind Tunnel Testing*, Wiley, New York, 1966.

[17]Scharpf, D. F., "An Experimental Investigation of Closely Coupled Tandem Wing Configurations at Low Reynolds Numbers," M.S. Thesis, University of Notre Dame, Notre Dame, IN, July 1989.

[18]Althaus, D., and Wortmann, F. X., *Stuttgarter Profilkatalog I*, Vieweg, Verlagsgesellschaft mbH, Braunschweig, 1981.

[19]Hoerner, S. F., *Fluid Dynamic Drag*, Hoerner, Great Britain, 1958, pp. 8–12.

Recommended Reading from the AIAA Progress in Astronautics and Aeronautics Series . . . AIAA

Dynamics of Explosions and Dynamics of Reactive Systems, I and II

J. R. Bowen, J. C. Leyer, and R. I. Soloukhin, editors

Companion volumes, *Dynamics of Explosions and Dynamics of Reactive Systems, I and II*, cover new findings in the gasdynamics of flows associated with exothermic processing—the essential feature of detonation waves—and other, associated phenomena.

Dynamics of Explosions (volume 106) primarily concerns the interrelationship between the rate processes of energy deposition in a compressible medium and the concurrent nonsteady flow as it typically occurs in explosion phenomena. *Dynamics of Reactive Systems* (Volume 105, parts I and II) spans a broader area, encompassing the processes coupling the dynamics of fluid flow and molecular transformations in reactive media, occurring in any combustion system. The two volumes, in addition to embracing the usual topics of explosions, detonations, shock phenomena, and reactive flow, treat gasdynamic aspects of nonsteady flow in combustion, and the effects of turbulence and diagnostic techniques used to study combustion phenomena.

Dynamics of Explosions
1986 664 pp. illus., Hardback
ISBN 0-930403-15-0
AIAA Members $54.95
Nonmembers $92.95
Order Number V-106

Dynamics of Reactive Systems I and II
1986 900 pp. (2 vols.), illus. Hardback
ISBN 0-930403-14-2
AIAA Members $86.95
Nonmembers $135.00
Order Number V-105

***TO ORDER:* Write, Phone, or FAX:** American Institute of Aeronautics and Astronautics c/o Publications Customer Service, 9 Jay Gould Ct., P.O. Box 753, Waldorf, MD 20604 Phone: 301/645-5643 or 1-800/682-AIAA, Dept. 415 ■ FAX: 301/843-0159

Sales Tax: CA residents, 8.25%; DC, 6%. For shipping and handling add $4.75 for 1–4 books (call for rates for higher quanties). Orders under $50.00 must be prepaid. Foreign orders must be prepaid. Please allow 4 weeks for delivery. Prices are subject to change without notice. Returns will be accepted within 15 days.